Thin Solid Films 574 (2015) 1–9

Contents lists available at ScienceDirect

Thin Solid Films

journal homepage: www.elsevier.com/locate/tsf

Graphene-wrapped ZnO nanospheres as a photocatalyst for high performance photocatalysis

Da Chen [a,*], Dongfang Wang [a], Qisheng Ge [a], Guangxing Ping [a], Meiqiang Fan [a,*], Laishun Qin [a], Liqun Bai [b], Chunju Lv [a], Kangying Shu [a]

[a] College of Materials Science & Engineering, China Jiliang University, Hangzhou 310018, China
[b] School of Sciences, Zhejiang Agriculture and Forestry University, Hangzhou 311300, China

ARTICLE INFO

Article history:
Received 12 December 2013
Received in revised form 13 November 2014
Accepted 13 November 2014
Available online 22 November 2014

Keywords:
Graphene
Zinc Oxide
Nanospheres
Lyophilization
Photocatalytic activity

ABSTRACT

In this work, graphene-wrapped ZnO nanospheres (ZnO–graphene nanocomposites) were prepared by a simple facile lyophilization method, followed by thermal treatment process. ZnO nanospheres with the size of about 100–400 nm, composed of numerous nanocrystals with hexagonal wurtzite structure, were well separated from each other and wrapped with transparent graphene sheets. Compared to ZnO nanospheres, the ZnO–graphene nanocomposites showed a significant enhancement in the photodegradation of methylene blue. This enhanced photocatalytic activity could be attributed to their favorable dye-adsorption affinity and increased optical absorption as well as the efficient charge transfer of the photogenerated electrons in the conduction band of ZnO to graphene. Thus, this work could provide a facile and low-cost method for the development of graphene-based nanocomposites with promising applications in photocatalysis, solar energy conversion, sensing, and so on.

1. Introduction

Organic dyes and their effluents have become one of the main sources of water pollution due to the great consumption in industry such as textile, paper, and plastic. Most of these dyes escape from traditional wastewater treatment and persist in water because of their high stability against light, temperature, and chemicals [1]. Recently, great interest has been stimulated in the treatment of organic contamination in water through photocatalytic method because it can destruct the pollutants completely and has a broad optional compound [2–4]. Photocatalysis is normally based on the light absorption of semiconductor oxide photocatalyst, typically TiO_2 or ZnO, to excite the electrons from valence band to conduction band and create electron-hole pairs. These photogenerated electrons and holes can migrate and initiate redox reactions with water and oxygen, and then degrade organic molecules absorbed on the surface of the photocatalyst [5]. Thus, semiconductor photocatalysis is deemed to an alternative technique to remove various organic pollutants.

ZnO, as a semiconductor, has been widely investigated as a photocatalyst material for photocatalytic degradation of the organic pollutants in natural environments because of its attractive photosensitivity and band gap, which can offer the high driving force for reduction and oxidation processes [6,7]. Despite its great potential, the photocatalytic efficiency of ZnO is often low because of the fast recombination of the photogenerated electron–hole pairs and the limited photoresponding range [2]. Therefore, various strategies, including structural design [8], noble metal loading [9], ion doping [10], and the coupling of semiconductors [11,12], have been proposed to extend the light absorption range or suppress the electron–hole recombination of ZnO. In particular, many works have been devoted to reduce the recombination of charge carriers by coupling ZnO with conjugative structure carbon materials, such as carbon nanotubes (CNTs) and C60 [13,14]. In a photocatalysis process, these carbon materials can act as an excellent electron-acceptor/transport material to effectively facilitate the migration of photo-induced electrons and hinder the charge recombination in electron-transfer processes due to the electronic interaction between ZnO and carbon materials, which enhances the photocatalytic performance.

As a rapidly rising star in carbon family, graphene, consisting of monolayers of carbon atoms arranged in a honeycombed network with six-membered rings, has generated increasing interest both in fundamental science and for wide potential applications due to its unique two-dimensional (2D) structure, excellent electronic properties, superior chemical stability, high specific surface area and high transparency [15,16]. Similar to the above mentioned carbon materials (such as CNTs or C60), graphene can also act as an excellent electron-acceptor/transport material [17]. More importantly, the combination of semiconductors and graphene may be an ideal system to accelerate the charge

* Corresponding authors. Tel.: +86 571 86835738; fax: +86 571 86835740.
E-mail addresses: dchen_80@hotmail.com (D. Chen), fanmeiqiang@126.com (M. Fan).

http://dx.doi.org/10.1016/j.tsf.2014.11.051
0040-6090/

transfer from photocatalyst to the liquid–solid interface contacting with organic pollutants by taking advantage of graphene's unique electron transport property [18]. Up to now, semiconductor nanomaterials such as TiO_2 and ZnO have been utilized to decorate graphene sheets to form graphene-supported nanomaterials with remarkable photocatalytic properties [17–20]. For example, Xu et al. [17] synthesized ZnO–graphene composite by reducing graphite oxide coated on the surface of commercial ZnO nanoparticles using hydrazine, and found that the ZnO–2 wt.% graphene composite showed a significantly improved photocatalytic efficiency (with the apparent reaction rate constant (k) of 0.098 min^{-1}) in the degradation of methylene blue (MB), which was about 4 times as that of pristine ZnO nanoparticles ($k = 0.022\ min^{-1}$). Although considerable advances in this area have already been made, the exploration on semiconductor oxide photocatalyst–graphene composites is not nearly enough so far. Especially, there are still some critical problems for the investigation of graphene as photocatalysts support. For example, the reduced graphene sheets tend to form irreversible agglomerates because of the van der Waals interaction and even restack to form graphite in the reduction from graphene oxide (GO) suspension solution or drying process [21]. The aggregation of graphene sheets will not only ruin the advantage of high surface area of graphene, but also obstruct the dispersion of semiconductor oxide particles. Thus, the development of effective approaches to prepare uniform semiconductor oxide–graphene hybrid photocatalysts is still a challenging topic in the photocatalysis research field.

In this work, we proposed and realized an optimized design of graphene-wrapped ZnO nanospheres (ZnO–graphene nanocomposites), consisting of ZnO nanospheres anchored on graphene sheets *via* a facile method, as schematically shown in Fig. 1. In this method, ZnO nanospheres were firstly prepared *via* a chemical solution route by refluxing their acetate precursors in diethylene glycol (DEG) at a relatively low temperature, and then the anchoring of ZnO nanospheres on graphene nanosheets was achieved by means of lyophilization followed by thermal reduction. The as-prepared ZnO–graphene nanocomposites were subsequently examined by various characterization techniques, and their photocatalytic performance was also evaluated by the photodegradation of methylene blue (MB). This work attempts to highlight the importance of the anchoring of ZnO nanospheres on graphene sheets for maximum utilization of ZnO photocatalyst and graphene as electron collector and transporter in photocatalytic degradation of organic pollutants.

2. Experimental section

2.1. Synthesis of ZnO nanospheres

The ZnO nanospheres were prepared by refluxing zinc acetate dihydrate (ZnAc) in DEG medium. Briefly, 0.025 mol ZnAc precursors and 0.5 mL of deionized water were added to 250 mL DEG, and the obtained solution was heated under reflux at 160 °C with stirring for 1 h. White ZnO precipitates were observed shortly after reaching the reaction temperature. Then, the resulting products were collected by centrifugation, rinsed by deionized water several times, and dried in an oven at 80 °C.

2.2. Synthesis of ZnO–graphene nanocomposites

Graphene oxide (GO) was produced from natural graphite powder by a modified Hummers' method as reported elsewhere [22]. The synthesis of ZnO–graphene nanocomposites was described as follows. Typically, 400 mg of ZnO nanospheres was added into the 80 mL GO aqueous suspension (0.5 mg/mL), and the obtained mixture was sonicated for 20 min to achieve a homogeneous black ZnO–GO suspension. Then, the resulting homogeneous aqueous suspension was lyophilized, followed by thermal reduction in a tube furnace with an atmosphere of 10% H_2 in N_2 at 700 °C for 2 h.

2.3. Materials characterizations

The morphologies of the samples were characterized by using a field-emission scanning electron microscope (FESEM, JEOL JSM-6700F, Japan) with an operating voltage of 15 kV and a transmission electron microscope (TEM, JEOL JEM-2100) using an operating voltage of 200 kV. The crystal phase identification of samples was performed on a X-ray diffraction (XRD) (Bruker Axs D2 PHASER, Germany) with Cu Kα radiation ($\lambda = 0.15406$ nm) at room temperature in the 2θ range from 10° to 80° with a step scan of 0.02°. Thermogravimetric

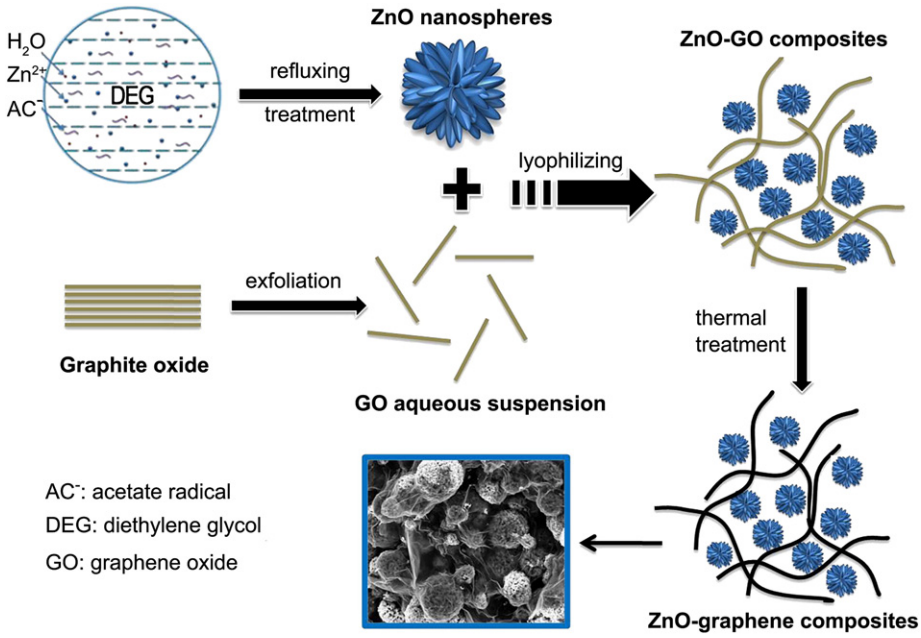

Fig. 1. Schematic illustration of the preparation of graphene-wrapped ZnO nanospheres.

analysis (TG) was carried out using a thermogravimetric analyzer (Mettler, SMP/PF7548/MET/600W, Switzerland) with a heating rate of 10 °C/min in air. The Fourier transform infrared (FTIR) absorption spectrum was obtained by FTIR spectrophotometer (Bruker Tensor 27, Germany). Raman spectra were collected by a Renishaw RM1000 microscope under ambient conditions, and the excitation wavelength was 514 nm. Specific surface areas were measured by Brunauer–Emmett–Teller nitrogen adsorption–desorption (Shimadzu, Micromeritics ASAP 2010 Instrument). The diffuse reflection spectra (DRS) were measured by a UV–vis spectrometer (Shimadzu Co. UV3600, Japan) equipped with integrating sphere accessory. A NQTM-AC-001 4294A Precision Impedance Analyzer was used to record the electrochemical impedance spectra (EIS) at room temperature over the frequency range of 30 MHz to 40 Hz with a 20 mV AC voltage perturbation.

2.4. Photoelectrochemical measurements

The aqueous suspensions of MB (5×10^{-5} M) were used as a model dye for the measurement of photocatalytic degradation. Prior to the photoelectrochemical measurements, the photocatalyst electrodes were firstly prepared on the F-doping SnO_2 conducting glass (FTO, 13 Ω/square, purchased from Sigma-Aldrich). The as-prepared sample (40 mg) was ultrasonicated in 2 mL of ethanol to disperse it evenly to get homogeneous suspension. The obtained paste was subsequently spread onto FTO glass whose side part was previously protected using Scotch tape. The as-prepared ZnO nanospheres or ZnO–graphene photoanodes were dried overnight at 200 °C in a muffle furnace, yielding a catalyst loading of ~0.6 mg/cm^2 on the FTO glass. Uncoated parts of the electrode were isolated with epoxy resin, and the film thickness measured with a profilometer was ca. 3 μm. In a typical photocatalytic process, MB solution and the as-prepared photocatalyst electrode were placed in a quartz-glass vessel. The photocatalyst and MB solution were allowed to stand in the dark for 30 min prior to illumination to allow for adsorption of MB onto the surface of the catalyst. The photoreaction vessel was then exposed to UV–vis irradiation under ambient conditions with an average intensity of 35 mW cm^{-2} produced by a 300-W Xenon lamp (XinGuang Technology Co., Ltd., Jiangsu, China), which was positioned 25 cm away from the vessel. The light source (Xenon lamp) shows a similar energy spectra distribution to the sunlight, covering the UV and visible ranges and part of the near IR range [23]. The irradiance intensity was measured by a radiometer (FZ-A, Photoelectric Instrument Factory of Beijing Normal University, China), and the temperature of photoreaction vessel could be controlled at ~25 °C by using a home-made circulating cooling water system. At given time intervals, the absorbance of MB solution was recorded with a 722 visible spectrophotometer (Cany Precision Instruments Co., Ltd., Shanghai, China) by recording variations of the maximum absorption band (662 nm) in the UV–vis spectrum of MB. All photodegradation experiments were repeated three times to check the reproducibility of the experimental results.

Photocurrent measurements were carried out using a CHI660D (CH Instruments, China) electrochemistry workstation in a conventional three-electrode system with the electrolyte solution of 0.1 M Na_2SO_4 under illumination, where the as-prepared ZnO or ZnO–graphene photoanode served as the working electrode, a platinum wire was used as the counter electrode, and Ag/AgCl was used as a reference electrode. A 300 W Xenon lamp (XinGuang Technology Co., Ltd., Jiangsu, China) was placed 25 cm away from the reaction vessel, which was used as the light source. The photoelectrochemical cell was illuminated from the FTO side of the ZnO or ZnO–graphene photoanode by incident light, and the illumination intensity on the photoanode was fixed at 35 mW/cm^2. The linear sweep voltammograms (the density current–voltage (J–V) curves) of the different samples under light illumination were recorded at a scan rate of 10 mV/s (with an applied potential from −0.5 to 0.5 V versus Ag/AgCl).

3. Results and discussion

3.1. Synthesis of graphene-wrapped ZnO nanospheres

The surface morphologies of the as-prepared ZnO nanospheres and ZnO–graphene nanocomposites were provided by FESEM images with different magnifications (Fig. 2). As shown in Fig. 2a, the as-prepared ZnO nanospheres had a typically spherical shape with diameters ranging from 100 to 400 nm, and didn't show macroscopic agglomeration. The enlarged FESEM image (Fig. 2b) further reveals that ZnO nanospheres were stacked with small nanoparticles standing out of the surface, thus making the surface of ZnO nanospheres rough and filled with irregular pores and small spikes. As for the as-prepared ZnO–graphene nanocomposites (Fig. 2c and d), it can be clearly observed that the ZnO nanospheres were well dispersed in the graphene framework with no obvious aggregation, and the majority of these ZnO nanospheres were wrapped with graphene nanosheets. In addition, the uniform mixture of ZnO nanospheres encapsulated by graphene is further demonstrated by the TEM images. Fig. 3 shows the TEM images of as-prepared ZnO nanospheres and ZnO–graphene nanocomposites. As shown, the as-prepared ZnO nanospheres (Fig. 3a) consisted of nearly uniform waxberry-like spheres with an average diameter of 200 nm, and each self-aggregated waxberry-like ZnO superstructure was made up of three-dimensionally spatially connected numerous fine nanocrystals. The high-resolution TEM (HRTEM) image of ZnO nanospheres (Fig. 3b) identified the lattice fringes with an interplanar distance of 0.28 nm, which could be assigned to the (100) plane of the hexagonal ZnO [5]. The typical TEM image of ZnO–graphene nanocomposites (Fig. 3c) reveals the hybridization structure of ZnO and graphene. As can be seen, ZnO nanospheres and 2D graphene sheets in the nanocomposites were clearly distinguished, and ZnO nanospheres were encapsulated by the wrinkled and transparent 2D graphene nanosheets. This indicates that the morphologies of ZnO nanospheres kept unchanged during the process of lyophilization and thermal reduction. Moreover, the HRTEM image (Fig. 3d) reveals the intimate contact between ZnO and graphene. It can be clearly seen that graphene nanosheets were coated on the surface of ZnO particles. The FESEM and TEM measurements demonstrated that the obtained graphene-wrapped ZnO nanospheres could form a three-dimensional (3D) network structure and provide an intimate contact between ZnO nanospheres and graphene nanosheets. This intimate contact makes possible the electronic interaction between ZnO and graphene, thus improving the charge separation and the photocatalytic activity of ZnO.

XRD measurements were employed to investigate the phase and structure of as-prepared ZnO nanospheres and ZnO–graphene nanocomposites. Fig. 4 shows the XRD patterns of as-prepared ZnO nanospheres and ZnO–graphene nanocomposites. For the as-prepared ZnO nanospheres, all diffraction peaks could be indexed to the hexagonal wurtzite phase structure of ZnO with lattice constants of a = 3.249 Å, c = 5.206 Å (JCPDS No. 36-1451) [24]. In contrast, ZnO–graphene nanocomposites showed a similar XRD pattern to that of pure ZnO nanospheres, and no any characteristic peak of graphite was observed, suggesting that the restacking of the as-reduced graphene sheets was effectively prevented [25]. The synthesis of ZnO–graphene nanocomposites was further confirmed by FTIR and Raman spectra. Fig. 5A shows the FTIR spectra of as-prepared graphene, GO, ZnO, ZnO–GO and ZnO–graphene nanocomposites, respectively. The oxygen-containing functional groups of GO were revealed by the bands at 1105, 1218, 1404 and 1725 cm^{-1} (curve b), corresponding to C–O stretching vibrations, C–OH stretching peak, C–O–H deformation peak and C═O stretching of COOH groups, respectively [26]. A strong and broad absorption at 3400 cm^{-1} could be assigned to the O–H stretching vibration of absorbed H_2O molecules, and the peak at

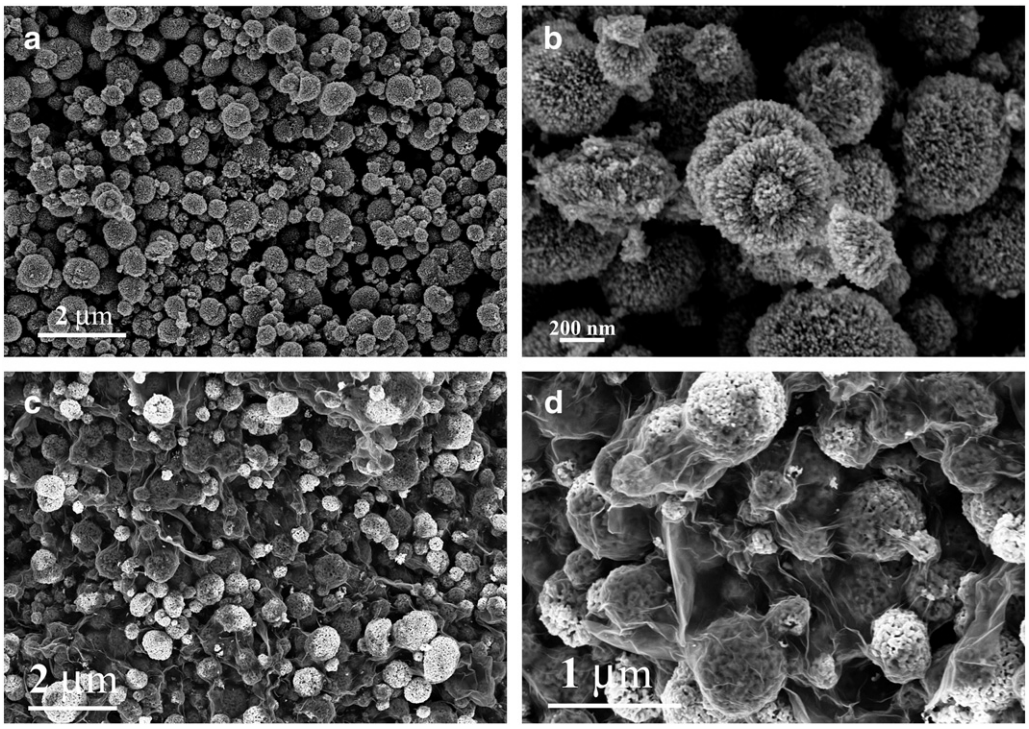

Fig. 2. FESEM images of as-prepared ZnO nanospheres at low (a) and high (b) magnification, and ZnO–graphene nanocomposites at low (c) and high (d) magnification.

1631 cm^{-1} could be assigned to the vibrations of the adsorbed water molecules and also the contributions from the skeletal vibrations of unoxidized graphitic domains [22]. For the graphene sample (curve a), the intensities of the bands associated to oxygen functional groups strongly decreased in relation to those of GO, and a peak at 1554 cm^{-1} attributed to aromatic C═C stretching vibration appeared

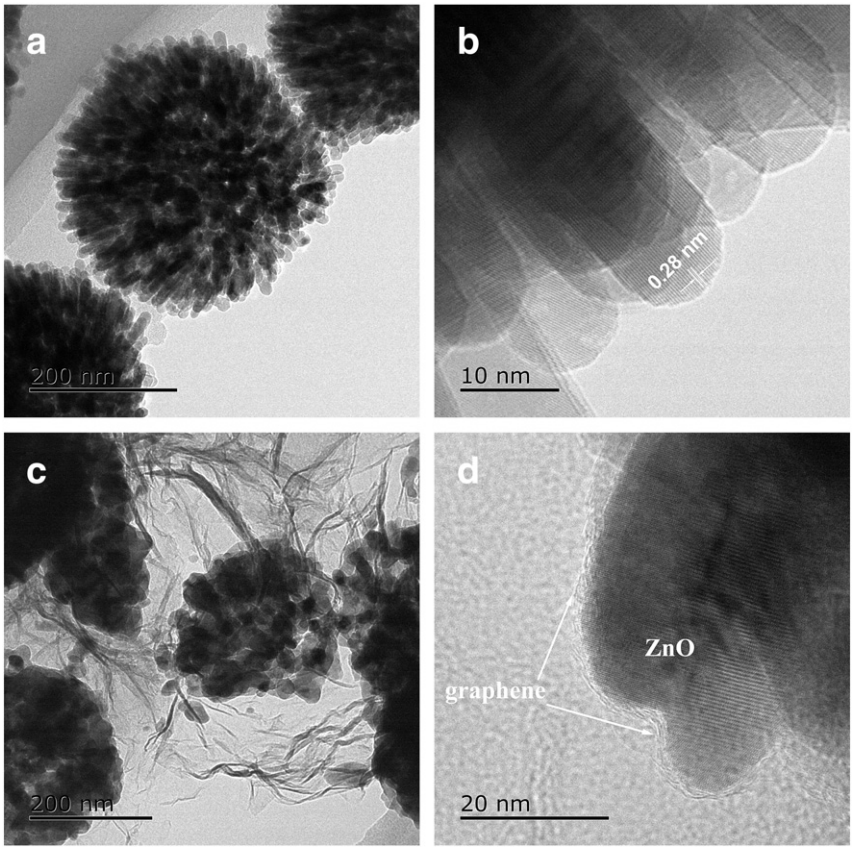

Fig. 3. Typical TEM images of as-prepared ZnO nanospheres (a) and ZnO–graphene nanocomposites (c); HRTEM images of as-prepared ZnO nanospheres (b) and ZnO–graphene nanocomposites (d), respectively.

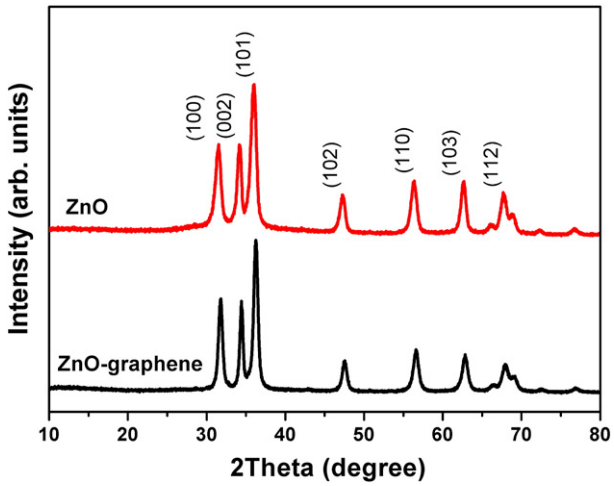

Fig. 4. XRD patterns of as-prepared ZnO nanospheres and ZnO–graphene nanocomposites.

[27]. As for ZnO nanospheres (curve c), the strong absorption band in the range of 410–565 cm^{-1} was attributed to the Zn – O stretching vibration of ZnO [28], and the two peaks at ~3400 and ~1617 cm^{-1} were attributed to the O – H stretching vibration and H – O – H bending vibration of the absorbed H_2O in ZnO nanospheres. For the as-prepared ZnO–GO and ZnO–graphene nanocomposites (curve d and e), all the characteristic peaks could be assigned to the above-mentioned bands of ZnO, GO or graphene. It can be seen that compared to those in GO and ZnO–GO, the intensities of the bands corresponding to the oxygen functional groups and O – H stretching vibration in ZnO–graphene decreased too much, suggesting the effective reduction of GO sheets by thermal treatment. The structural changes of the as-prepared GO, ZnO–GO nanocomposites and ZnO–graphene nanocomposites are investigated by the Raman spectroscopy (shown in Fig. 5B), which is a suitable technique to study the ordered/disordered crystal structures of graphitic materials. The spectrum of GO exhibited the characteristic *G*-band (1598 cm^{-1}) and *D*-band (1349 cm^{-1}) with a *D* to *G* intensity ratio of about 1.044. The *G*-band arises from the vibration of the sp^2 bonded carbon atoms and the *D*-band is attributed to structural disorder at defect sites with the *D*/*G* ratio usually taken as a measure of the quality of the graphitic structures [29]. The Raman spectra of ZnO–GO and ZnO–graphene nanocomposites showed similar *G* and *D* bands structure of carbon, suggesting that the structure of graphene was maintained in the nanocomposites. The peak at 328 cm^{-1} could be assigned to the $2E_2$ (*M*) mode of ZnO, and the one at 437 cm^{-1} corresponds to the E_2 (*high*) vibration mode of ZnO [30]. It is worth noting that a measurable G band shift from 1598 to 1587 cm^{-1} was observed for ZnO–graphene compared with GO and ZnO–GO. This band shift was generally given as an indicator for GO reduction [17,30]. Further, the calculated I_D/I_G (intensity ratio of the *D* and *G* bands) values of GO, ZnO–GO and ZnO–graphene were 1.044, 1.015 and 0.867, respectively. The decrease of the I_D/I_G ratio in the ZnO–graphene nanocomposites suggests an increase in the average size of the sp^2 domains and the restoration of conjugation in the aromatic carbon atoms by removal of oxygenated groups upon the thermal treatment process. Based on the above observations, it can be concluded that ZnO–GO could be effectively reduced to ZnO–graphene *via* the thermal treatment process.

To determine the content of graphene in the ZnO–graphene nanocomposites, TG measurements were performed in air from 50 °C to 800 °C. Fig. 6 shows the TG curves of GO, ZnO nanospheres, ZnO–GO and ZnO–graphene nanocomposites. As shown, ZnO nanospheres exhibited good thermal stability in the whole thermal process. For the sample of GO, a small weight loss (13 wt.%) at around 150 °C and a major weight loss (24 wt.%) at around 220 °C were found, which could be ascribed to the loss of adsorbed water and pyrolysis of the labile oxygen-containing functional groups, respectively, while the largest weight loss occurs at around 550 °C due to the complete oxidation reaction of GO. Thus, it is reasonable to determine the content of GO or graphene in the nanocomposites from the largest weight loss in the TG curves of ZnO–GO or ZnO–graphene nanocomposites. Therefore,

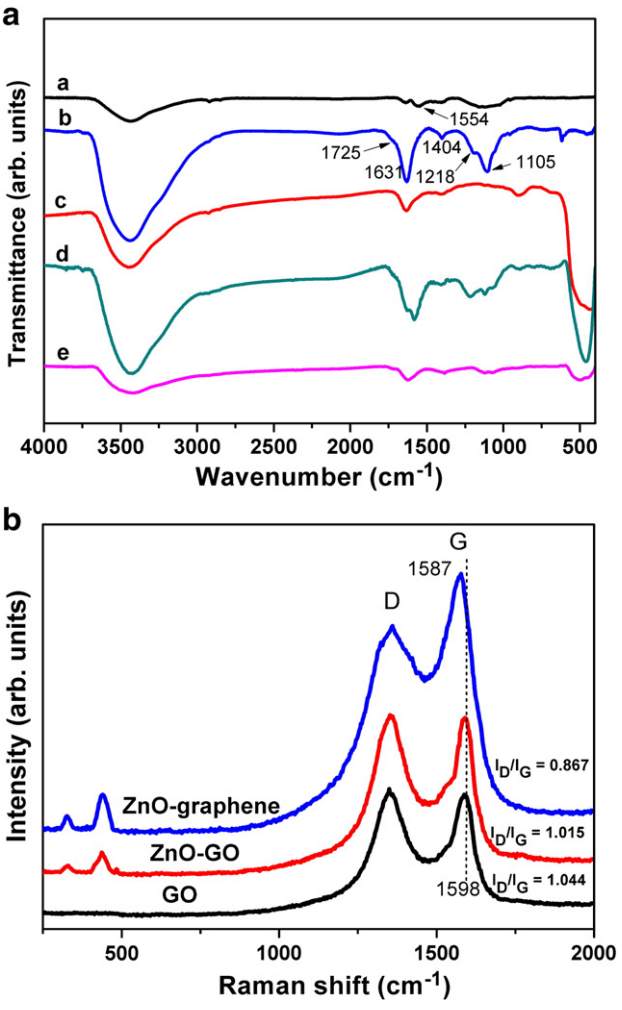

Fig. 5. (A) FTIR spectra of as-prepared (a) graphene, (b) GO, (c) ZnO nanospheres, (d) ZnO–GO nanocomposites and (e) ZnO–graphene nanocomposites; (B) Raman spectra for as-prepared GO, ZnO–GO and ZnO–graphene anocomposites.

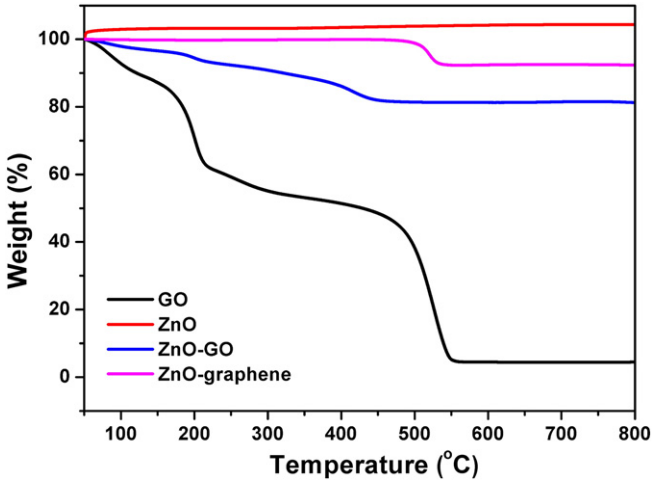

Fig. 6. The TG curves of as-prepared GO, graphene, ZnO nanospheres, ZnO–GO nanocomposites and ZnO–graphene nanocomposites.

the content of GO in ZnO–GO nanocomposites was estimated to be 8.6 wt.%, which was on the whole consistent with the feed ratio of GO (9.1 wt.%). The content of graphene, however, was calculated to be 7.2 wt.%. Obviously, this value was lower than that of GO in ZnO–GO nanocomposites due to the partial removal of oxygen-containing functional groups during the thermal reduction.

3.2. Photocatalytic activities

The photocatalytic activities of the as-prepared ZnO nanospheres and ZnO–graphene nanocomposites were evaluated by measuring the decomposition of MB as a model reaction. Fig. 7A shows the temporal concentration changes of MB solution without any catalyst, or catalyzed by the as-prepared ZnO nanospheres and ZnO–graphene nanocomposites under light irradiation, respectively. As shown, there was no significant degradation of the dye solution without the catalyst after 140 min light irradiation, indicating that the discoloration of MB solution under light irradiation could be neglected. A satisfactory fitting was clearly observed in photodegradation processes with the catalysts, confirming the quasi-first-order-type kinetics. It was evidenced by the linear plot of $\ln(C/C_0)$ versus reaction time, $-\ln(C/C_0) = Kt$, where K was the rate constant of the degradation. In this case, K was calculated to be 0.812%, 1.15% min^{-1} for the ZnO nanospheres and ZnO–graphene nanocomposites, respectively. Apparently, the photocatalytic activity of ZnO–graphene nanocomposites was higher than that of ZnO nanospheres. In addition, the reproducibility and repeatability of photocatalytic activities of as-prepared ZnO nanospheres and ZnO–graphene nanocomposites were evaluated. For each sample, three trials of the MB photodegradation process were performed under light irradiation for 140 min, and the experimental results are summarized in Table 1. As can be seen, these trials had good agreement, with 66.6%, 65.9%, and 67.2% of MB removal for ZnO nanospheres, and with 81.9%, 83.3% and 82.5% of MB removal for ZnO–graphene nanocomposites, respectively. This indicates that both ZnO nanospheres and ZnO–graphene nanocomposites had excellent reproducibility. Further, the photocatalysts of ZnO nanospheres and ZnO–graphene nanocomposites were recycled for consecutive photodegradation of MB aqueous solution (5×10^{-5} M), and the process was repeated up to five times. The efficiencies of the photodegradation processes were evaluated and compared between the reuse cycles for each sample, as shown in Fig. 7B. It can be seen that with the increase of the reuse cycle, the degradation rate of each sample (ZnO nanospheres or ZnO–graphene nanocomposites) decreased gradually. The MB photodegradation rate of ZnO nanospheres after five reuse cycles was 76.4% of the initial rate, while ZnO–graphene nanocomposites after five reuse cycles still retained 89.6% activity for degradation of MB. These studies revealed that the as-prepared photocatalysts of ZnO nanospheres and ZnO–graphene nanocomposites demonstrated good stability, and ZnO–graphene nanocomposites exhibited much higher reusability than ZnO nanospheres.

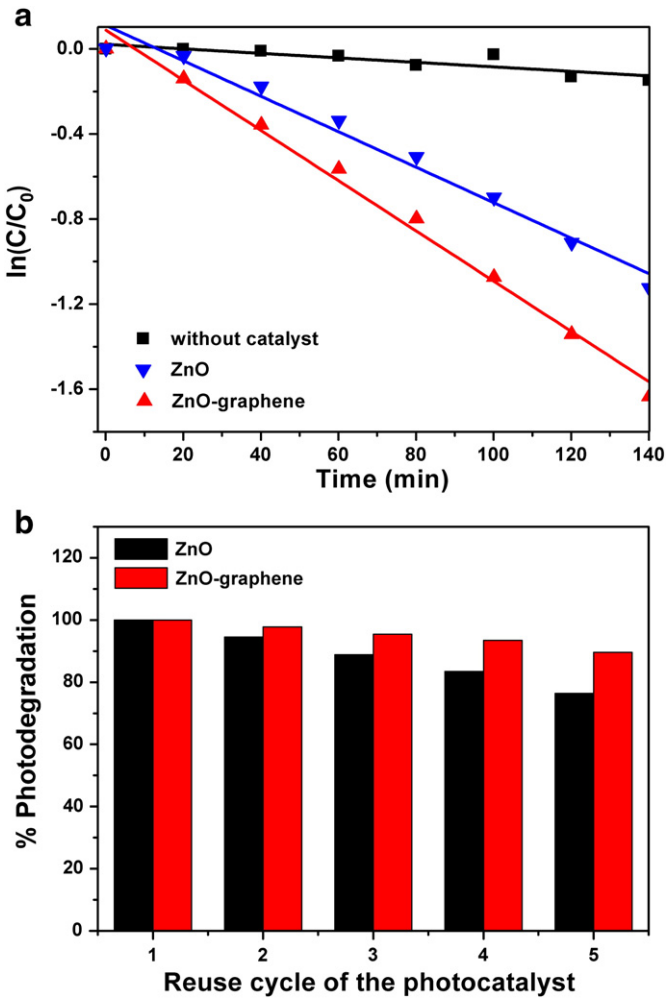

Fig. 7. (A) Absorption changes ($\lambda = 662$ nm) plot for the photocatalytic degradation of methylene blue (MB) aqueous solution and the solution with the as-prepared ZnO nanospheres and ZnO–graphene nanocomposites. (C/C_0 is the normalized concentration of the solution). (B) The variation of photocatalytic degradation rate of the as-prepared ZnO nanospheres and ZnO–graphene nanocomposites as a function of reuse cycle.

The enhanced photocatalytic activity of ZnO–graphene nanocomposites could be attributed to the following reasons. One is the comparatively large surface area which is related to the crystal size and/or morphology of the photocatalyst. It is generally believed that the larger specific surface area the photocatalysts own, the higher adsorption of target molecules and ability of generating photoinduced electron–hole pairs of active sites it has [31,32]. In the present work, ZnO nanospheres had a larger surface area (34.157 m^2/g) than that of the ZnO–graphene nanocomposites (22.354 m^2/g). However, the adsorption measurements (as summarized in Table 1) revealed that ZnO–graphene nanospheres showed more than 24% of MB adsorption after reaching adsorption–desorption equilibrium in dark for 30 min, which was much larger than that of ZnO nanospheres (less than 10%). The fact that surface area and the adsorption ability as well as photoactivity followed opposite trends should alert one that the surface area was not the only factor responsible for determining the adsorption affinity and photoactivity of ZnO–graphene nanocomposites. In our case, the higher adsorption of MB molecules onto the ZnO–graphene nanocomposites could be ascribed to the π–π stacking between MB and the π-conjugation regions of the graphene nanosheets in the nanocomposites, which could contribute much to the noncovalent adsorption of dye molecules [33], thus leading to the enhanced photocatalytic activities.

Table 1
Summary on the reproducibility measurements of MB photodegradation under light irradiation after 140 min for as-prepared ZnO nanospheres and ZnO–graphene nanocomposites, and the amount of adsorbed MB onto the photocatalysts of ZnO nanospheres or ZnO–graphene nanocomposites after reaching adsorption-desorption equilibrium in dark for 30 min.

Photocatalyst	Trial No.	Amount of absorbed MB (%)	MB removal (%)	Degradation rate constant (K), (min^{-1})
ZnO nanospheres	1	9.2	66.6	0.812%
	2	7.7	65.9	0.785%
	3	8.5	67.2	0.834%
ZnO–graphene nanocomposites	1	24.6	81.9	1.158%
	2	26.9	83.3	1.272%
	3	25.4	82.5	1.216%

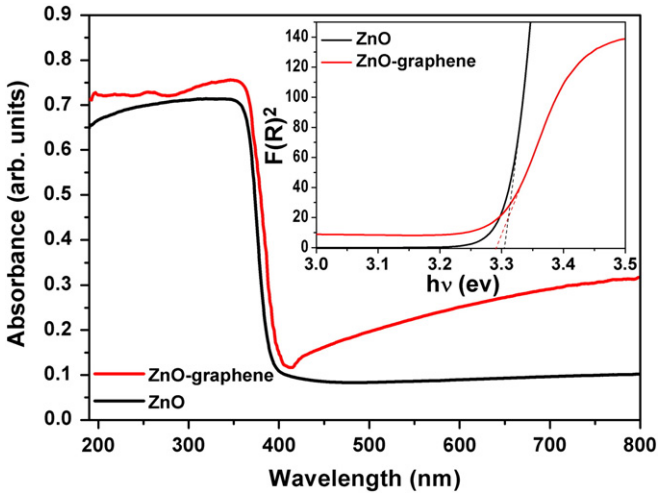

Fig. 8. Diffuse reflectance absorption spectra of as-prepared ZnO nanospheres and ZnO–graphene nanocomposites (inset: the plot of $F(R)^2$ versus photon energy of as-prepared ZnO nanospheres and ZnO–graphene nanocomposites).

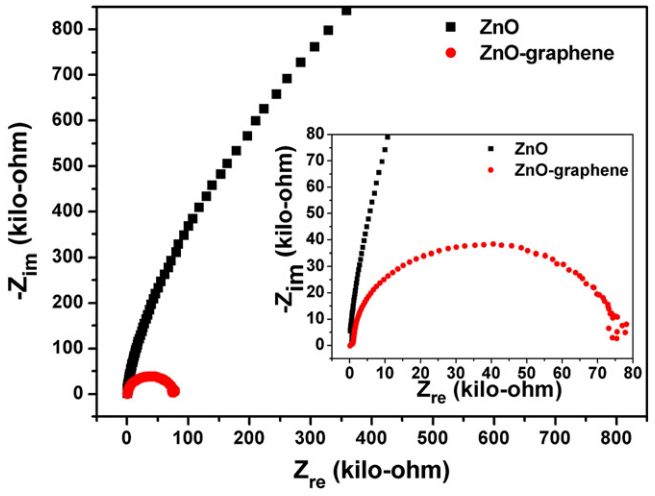

Fig. 9. Nyquist plots of ZnO nanospheres and ZnO–graphene nanocomposites from 30 MHz to 40 Hz.

Another crucial factor contributing to the enhanced photocatalytic activity of ZnO–graphene nanocomposites is the enhanced optical absorption in the UV–visible region. To reveal the optical absorption abilities of as-prepared ZnO nanospheres and ZnO–graphene nanocomposites in the UV–vis region, DRS measurements were performed. Fig. 8 shows the UV–vis diffuse reflectance absorption spectra of as-prepared ZnO nanospheres and ZnO–graphene nanocomposites. It can be seen that the absorption edge of ZnO nanospheres was at about 380 nm, and no apparent absorption was observed in the visible-light region, which coincide with the literature [34]. After introduction of graphene, the ZnO–graphene nanocomposites underwent a red shift and an enhanced optical absorption both in ultraviolet region and visible region. Further, the band-gap energies of as-prepared ZnO nanospheres and ZnO–graphene nanocomposites, which can be determined by plotting the square of the Kubelka–Munk function $F(R)^2$ vs. energy [35], were calculated to be 3.31 eV and 3.29 eV (as shown in the inset of Fig. 8), respectively. The band-gap energy of ZnO–graphene nanocomposites was reduced very slightly compared to that of ZnO nanospheres. This means that the slightly-reduced band-gap energy probably had very little effect on the enhanced optical absorption of ZnO–graphene nanocomposites in the UV–visible region. Therefore, the enhanced absorption ability of this nanocomposite could be mainly attributed to the introduction of black body properties typical of graphite-like materials (i.e., graphene) [17] and the synergistic effects between graphene and ZnO nanospheres. Obviously, ZnO–graphene nanocomposites possessed a stronger light absorption than ZnO nanospheres, implying it possibly behaves an enhanced photocatalytic activity.

In addition, similar to other carbonaceous materials (such as: CNTs and graphite-like carbon) in the coupling of the photocatalysts [14,36], graphene could also act as electron scavenging agents and serve as an electrical conducting network for electron transfer in ZnO–graphene nanocomposites, which would promote interfacial charge transfer and decrease the quick recombination of photo-generated charge carriers. To investigate the charge transport properties of as-prepared ZnO nanospheres and ZnO–graphene nanocomposites, EIS measurements were performed. Fig. 9 shows the Nyquist plots of the impedance data of as-prepared ZnO nanospheres and ZnO–graphene nanocomposites, in which a typical complex-plane plot of imaginary impedance versus real impedance was plotted to analyze their corresponding charge transfer resistance. As known, the impedance spectra generally include a semicircle portion, observed at higher frequencies, that corresponds to the kinetic control of the charge-transfer process, followed by a linear part characteristic of the lower frequency attributable to the diffusion process [37]. In the present work, it could be observed that the semicircle of ZnO–graphene nanocomposites in the plot was much smaller than that of ZnO nanospheres, indicating that the charge transfer resistance of ZnO–graphene nanocomposites was significantly decreased compared to that of ZnO nanospheres. The improved conductivity could be ascribed to the high conductivity of graphene as well as the intimate contact between ZnO and graphene, which could facilitate the transfer of excited electrons from the ZnO conduction band to graphene *via* a percolation mechanism possible, and thereby the efficient separation of the photo-induced electrons and the hindrance of the charge recombination in electron-transfer processes. In order to further investigate the electronic interaction between ZnO and graphene, the photocurrent measurements for ZnO and ZnO–graphene electrodes as photoanodes were performed in a three-electrode system under illumination. The linear sweep voltammograms (*J–V* curve) are illustrated in Fig. 10A, which describes the photocurrent potential characteristics of as-prepared ZnO nanospheres and ZnO–graphene nanocomposites. It is easy to find that both ZnO and ZnO–graphene electrodes display anodic photocurrent corresponding to the n-type photoresponse [17], and the anodic photocurrent increased with the increase of bias potential (versus Ag/Ag/Cl). The ZnO–graphene composite photoanode shows the highest photocurrent density, around 1.62 mA/cm^2 at 0.5 V bias versus Ag/AgCl, which is observed to be 4 fold more compared to ZnO photoanode (0.39 mA/cm^2). Moreover, the photoinduced behavior of the generated photocurrent from ZnO and ZnO–graphene photoanodes at 0 V bias versus Ag/AgCl is shown in Fig. 10B. When the light was regularly switched on and off, a series of almost identical electric signals could be obtained. It is worthy to note that the photocurrent of ZnO–graphene photoanode (0.074 mA/cm^2) was about 3–4 times as high as that of the ZnO photoanode (0.019 mA/cm^2), and the photocurrent was so stable that no obvious photocurrent decay was observed. It is clear that the photocurrent of ZnO–graphene composite photoanode was greatly improved when compared to that of ZnO photoanode. The enhanced anodic photocurrent of ZnO–graphene electrode was considered to be contributed to the two factors: (i) the higher separation efficiency of the photoinduced electron-hole pairs and lower recombination rate from the interaction of ZnO and graphene, and (ii) the decrease in the solid-state interface layer resistance and the charge transfer resistance on the surface, which was demonstrated by the above electrochemical impedance measurements. Thus, the improved separation efficiency and the decreased recombination rate of the photoinduced electron-hole pairs as well as the decreased charge-transfer resistance should be another reasonable explanation for the enhanced photocatalytic activities of ZnO–graphene nanocomposites.

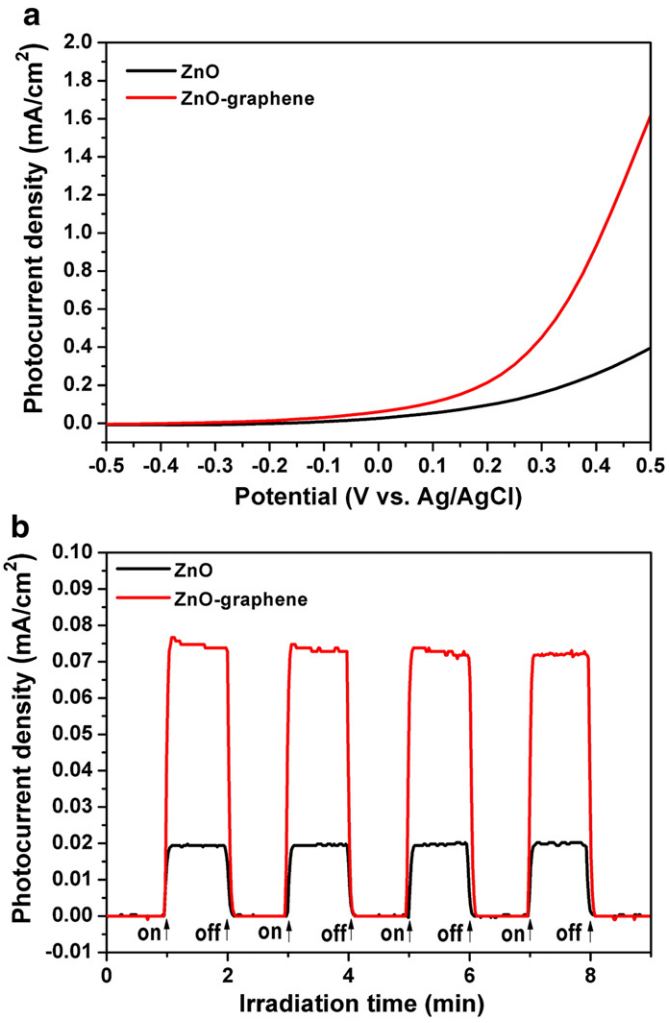

Fig. 10. (A) Linear sweep voltammograms (*J–V* curves) obtained from ZnO nanospheres and ZnO–graphene nanocomposites in 0.1 M Na_2SO_4 electrolyte solution under light irradiation; and (B) time-resolved photocurrent generation with illumination toggling between "on" and "off" for the ZnO and ZnO–graphene photoanodes at 0 V bias versus Ag/AgCl.

4. Conclusions

In summary, graphene-wrapped ZnO nanospheres were prepared through a facile lyophilization method, followed by thermal treatment process. The as-prepared ZnO–graphene nanocomposites were characterized by FESEM, TEM, XRD, FTIR and TG measurements. Experimental results showed that ZnO nanospheres with the diameters of about 100–400 nm, which were composed of numerous nanocrystals with hexagonal wurtzite structure, were well dispersed in the graphene framework, and the majority of ZnO nanospheres were wrapped with graphene sheets. The wrapping of ZnO with graphene could form a 3D network structure and provide an intimate contact between ZnO nanospheres and graphene nanosheets. In addition, the photocatalytic activity of ZnO–graphene nanocomposites was demonstrated to be significantly higher than that of ZnO nanospheres. The enhanced photocatalytic activity of ZnO–graphene nanocomposites could be attributed to their favorable dye-adsorption affinity and increased optical absorption as well as the efficient charge transfer of the photogenerated electrons in the conduction band of ZnO to graphene. Thus, the present work provides a facile and low-cost pathway to prepare ZnO–graphene composite photocatalysts with promising applications in photocatalysis, solar energy conversion, sensing, and so on.

Acknowledgments

This work was financially supported by the National Natural Science Foundation of China (Nos. 21003111, 51372237, and 11175169), the International S&T Cooperation Program of China (No. 2013DFG52490), and the research fund of the Key Laboratory for Advanced Technology in Environmental Protection of Jiangsu Province (AE201304).

References

[1] H.S. Rai, M.S. Bhattacharyya, J. Singh, T.K. Bansal, P. Vats, U.C. Banerjee, Removal of dyes from the effluent of textile and dyestuff manufacturing industry: a review of emerging techniques with reference to biological treatment, Crit. Rev. Environ. Sci. Technol. 35 (2005) 219.
[2] M.R. Hoffmann, S.T. Martin, W.Y. Choi, D.W. Bahnemannt, Environmental applications of semiconductor photocatalysis, Chem. Rev. 95 (1995) 69.
[3] U.I. Gaya, A.H. Abdullah, Heterogeneous photocatalytic degradation of organic contaminants over titanium dioxide: a review of fundamentals, progress and problems, J. Photochem. Photobiol. C Photochem. Rev. 9 (2008) 1.
[4] J.H. Li, J.Z. Zhang, Optical properties and applications of hybrid semiconductor nanomaterials, Coord. Chem. Rev. 253 (2009) 3015.
[5] T. Lv, L.K. Pan, X.J. Liu, T. Lu, G. Zhu, Z. Sun, Enhanced photocatalytic degradation of methylene blue by ZnO-reduced graphene oxide composite synthesized via microwave-assisted reaction, J. Alloys Compd. 509 (2011) 10086.
[6] A.K. Sinha, M. Basu, M. Pradhan, S. Sarkar, T. Pal, Fabrication of large-scale hierarchical ZnO hollow spheroids for hydrophobicity and photocatalysis, Chem. Eur. J. 16 (2010) 7865.
[7] L.N. Wang, Y.Y. Zheng, X.Y. Li, W.J. Dong, W.H. Tang, B.Y. Chen, C.R. Li, X. Li, T.R. Zhang, W. Xu, Nanostructured porous ZnO film with enhanced photocatalytic activity, Thin Solid Films 519 (2011) 5673.
[8] Y. Wu, M.H. Huang, H. Feick, N. Tran, E. Weber, P. Yang, Catalytic growth of zinc oxide nanowires by vapor transport, Adv. Mater. 13 (2001) 113.
[9] W. Xie, Y.Z. Li, W. Sun, J.C. Huang, H. Xie, X.J. Zhao, Surface modification of ZnO with Ag improves its photocatalytic efficiency and photostability, J. Photochem. Photobiol. A Chem. 216 (2010) 149.
[10] H.C. Qin, W.Y. Li, Y.J. Xia, T. He, Photocatalytic activity of heterostructures based on ZnO and N-doped ZnO, ACS Appl. Mater. Interfaces 3 (2011) 3152.
[11] C. Wang, X.M. Wang, B.Q. Xu, J.C. Zhao, B.X. Mai, P.A. Peng, G.Y. Sheng, J.M. Fu, Enhanced photocatalytic performance of nanosized coupled ZnO/SnO_2 photocatalysts for methyl orange degradation, J. Photochem. Photobiol. A Chem. 168 (2004) 47.
[12] D. Chen, H. Zhang, S. Hu, J.H. Li, Preparation and enhanced photoelectrochemical performance of coupled bicomponent $ZnO–TiO_2$ nanocomposites, J. Phys. Chem. C 112 (2008) 117.
[13] H.B. Fu, T.G. Xu, S.B. Zhu, Y.F. Zhu, Photocorrosion inhibition and enhancement of photocatalytic activity for ZnO via hybridization with C60, Environ. Sci. Technol. 42 (2008) 8064.
[14] K. Woan, G. Pyrgiotakis, W. Sigmund, Photocatalytic carbon-nanotube–TiO_2 composites, Adv. Mater. 21 (2009) 2233.
[15] D. Li, R.B. Kaner, Graphene-based materials, Science 320 (2008) 1170.
[16] D. Chen, L.H. Tang, J.H. Li, Graphene-based materials in electrochemistry, Chem. Soc. Rev. 39 (2010) 3157.
[17] T.G. Xu, L.W. Zhang, H.Y. Cheng, Y.F. Zhu, Significantly enhanced photocatalytic performance of ZnO via graphene hybridization and the mechanism study, Appl. Catal. B Environ. 101 (2011) 382.
[18] Y. Liu, Y. Hu, M.J. Zhou, H.S. Qian, X. Hu, Microwave-assisted non-aqueous route to deposit well-dispersed ZnO nanocrystals on reduced graphene oxide sheets with improved photoactivity for the decolorization of dyes under visible light, Appl. Catal. B Environ. 125 (2012) 425.
[19] H. Zhang, X.J. Lv, Y.M. Li, Y. Wang, J.H. Li, P25–graphene composite as a high performance photocatalyst, ACS Nano 4 (2010) 380.
[20] B.J. Li, H.Q. Cao, ZnO@graphene composite with enhanced performance for the removal of dye from water, J. Mater. Chem. 21 (2011) 3346.
[21] C. Xu, X. Wang, J.W. Zhu, Graphene–metal particle nanocomposites, J. Phys. Chem. C 112 (2008) 19841.
[22] Y.X. Xu, H. Bai, G.W. Lu, C. Li, G.Q. Shi, Flexible graphene films via the filtration of water-soluble noncovalent functionalized graphene sheets, J. Am. Chem. Soc. 130 (2008) 5856.
[23] Q. Jing, W.Y. Fu, W.C. Li, H.B. Yang, M.H. Li, J.W. Ma, X.M. Zhou, M.L. Sun, H. Zhao, Y.Y. Zhang, W.Y. Zhao, L.N. Zhang, H. Chen, Synthesis of snowflake-like multi-layered ZnO with controllable pore sizes and its photocatalytic property, Appl. Surf. Sci. 258 (2012) 3604.
[24] B. Liu, H.C. Zeng, Hydrothermal synthesis of ZnO nanorods in the diameter regime of 50 nm, J. Am. Chem. Soc. 125 (2003) 4430.
[25] D.Y. Cai, M. Song, Preparation of fully exfoliated graphite oxide nanoplatelets in organic solvents, J. Mater. Chem. 17 (2007) 3678.
[26] J.L. Wu, X.P. Shen, L. Jiang, K. Wang, K.M. Chen, Solvothermal synthesis and characterization of sandwich-like graphene/ZnO nanocomposites, Appl. Surf. Sci. 256 (2010) 2826.
[27] C. Nethravathi, M. Rajamathi, Chemically modified graphene sheets produced by the solvothermal reduction of colloidal dispersions of graphite oxide, Carbon 46 (2008) 1994.

[28] F. Gu, S.F. Wang, M.K. Lü, G.J. Zhou, D. Xu, D.R. Yuan, Structure evaluation and highly enhanced luminescence of Dy^{3+}-doped ZnO nanocrystals by Li^{+} doping via combustion method, Langmuir 20 (2004) 3528.
[29] H.T. Liu, L. Zhang, Y.L. Guo, C. Cheng, L.J. Yang, L. Jiang, G. Yu, W.P. Hu, Y.Q. Liu, D.B. Zhu, Reduction of graphene oxide to highly conductive graphene by Lawesson's reagent and its electrical applications, J. Mater. Chem. C 1 (2013) 3104.
[30] Z.Y. Zhan, L.X. Zheng, Y.Z. Pan, G.Z. Sun, L. Li, Self-powered, visible-light photodetector based on thermally reduced graphene oxide–ZnO (rGO–ZnO) hybrid nanostructure, J. Mater. Chem. 22 (2012) 2589.
[31] S.Y. Chae, M.K. Park, S.K. Lee, T.Y. Kim, S.K. Kim, W.I. Lee, Preparation of size-controlled TiO_2 nanoparticles and derivation of optically transparent photocatalytic films, Chem. Mater. 15 (2003) 3326.
[32] M.A. Carreon, S.Y. Choi, M. Mamak, N. Choprab, G.A. Ozin, Pore architecture affects photocatalytic activity of periodic mesoporous nanocrystalline anatase thin films, J. Mater. Chem. 17 (2007) 82.
[33] Z. Liu, J.T. Robinson, X.M. Sunand, H.J. Dai, PEGylated nanographene oxide for delivery of water-insoluble cancer drugs, J. Am. Chem. Soc. 130 (2008) 10876.
[34] W.J. Han, L. Ren, X. Qi, Y.D. Liu, X.L. Wei, Z.Y. Huang, J.X. Zhong, Synthesis of CdS/ZnO/graphene composite with high-efficiency photoelectrochemical activities under solar radiation, Appl. Surf. Sci. 299 (2014) 12.
[35] G. Cao, L.K. Rabenberg, C.M. Nunn, T.E. Mallouk, Formation of quantum-size semiconductor particles in a layered metal phosphonate host lattice, Chem. Mater. 3 (1991) 149.
[36] L.W. Zhang, H.Y. Cheng, R.L. Zong, Y.F. Zhu, Photocorrosion suppression of ZnO nanoparticles via hybridization with graphite-like carbon and enhanced photocatalytic activity, J. Phys. Chem. C 113 (2009) 2368.
[37] B.Y. Chang, S.M. Park, Electrochemical impedance spectroscopy, Annu. Rev. Anal. Chem. 3 (2010) 207.